JOINT EUROPEAN TORUS

JET–P(92)98

L-G Eriksson, P. Helander
and JET Team

Finite Orbit-Width Effects on Stochastic Ripple Diffusion

Finite Orbit-Width Effects on Stochastic Ripple Diffusion

L-G Eriksson, P. Helander[1] and JET Team*

JET-Joint Undertaking, Culham Science Centre, OX14 3DB, Abingdon, UK

[1] *Institute for Electromagnetic Field Theory and Plasma Physics, Chalmers University of Technology, Goteborg, Sweden*
** See Annex*

Preprint of Paper to be submitted for publication in
Nuclear Fusion

ABSTRACT.

An analytical and numerical investigation is undertaken to study the effects of non- standard orbit topology on stochastic ripple diffusion of high-energy ions in tokamaks. Finite orbit-width effects are demonstrated to lead to large modifications of the threshold for the onset of stochastic motion. Trapped particles moving along trajectories with turning points on the inside of the torus are most severely affected. In particular, orbits close to the pinch orbit are very sensitive to magnetic field ripple, whereas orbits with bounce points close to the horizontal midplane are less easily perturbed than suggested by small orbit-width theory. Applying the results to recent ripple experiments on JET, we find that the number of stochastically moving particles is only moderately affected by these effects. The reason for this is the large ripple amplitude and the steepness of ripple gradient over most of the plasma cross section.

I. Introduction

The possibility of α-particles being subject to stochastic ripple diffusion imposes a rather severe restriction on the acceptable toroidal field ripple in a tokamak reactor [1]. It is therefore important to test the validity of theoretical predictions by performing ripple experiments in existing tokamaks. Recently, such experiments have been carried out on JET [2] and TFTR [3]. When comparing the results of such experiments with theory one has to take care. Because of their high energy and the low magnetic field (compared with that in a reactor), many of the particles suffering stochastic ripple diffusion in the above mentioned experiments do not follow the magnetic field lines. Instead, they move along very wide, non-standard orbits, i.e. along orbits which are not adequately described by the usual small banana-width approximation. However, much of the existing theory is based on the assumption of small banana-width, and it is not evident that such theories are applicable for non-standard orbits.

In the small banana-width limit, the theory of stochastic ripple diffusion is well developed, see, e.g. Refs [1,4,5,6]. If the ripple amplitude exceeds some certain threshold so that particle orbits become chaotic, very rapid losses of fusion-generated α-particles and other fast ions occur. In this paper, we examine the influence of non-standard orbit topology on the stochastization threshold. We find that there are two main types of orbits for which this is important. First, for ions with non-standard orbits close to the so-called pinch orbit [7], the stochastization threshold becomes very small. The trapped ions which are subject to this effect have their turning points on the high-field side of the torus. Second, for trajectories with their turning points close to the horizontal midplane, the stochastization threshold tends to be grossly underestimated by small banana-width theory. As a result of these two effects, the threshold value resulting from our and previous calculations differ by as much as two orders of magnitude in either direction. We do not consider other ripple transport mechanisms, such as trapping in local magnetic wells and collisional ripple diffusion.

Numerical simulations of stochastic ripple diffusion using particle-following codes were reported in, e.g., Refs [8]-[9]. However, these deal with reactor-relevant cases, where the banana width indeed is small, and are therefore not immediately applicable to present-day tokamaks. Putvinskii has recently carried out simulations relevant to JET [10], but no detailed analysis of orbit-wdith effects was made.

In the recent ripple experiments on JET, a fairly large ripple was created by using only 16 of the 32 available toroidal field coils [2]. Ripple effects on both neutral beam injected ions and ions accelerated by ion cyclotron resonance heating (ICRH) were studied. In the case of ICRH, hydrogen minority ions were heated at the second harmonic of the cyclotron frequency to energies in the MeV range. Since the toroidal magnetic field was kept low (1.4 T), most of the hot ions acquired non-standard orbits in these discharges. It is therefore important for the interpretation of the ICRH ripple experiments on JET to understand how ions with non-standard orbits are affected by the ripple. For this reason, we have chosen to apply our results for JET-relevant cases.

The paper is organized as follows: In Section II, we solve the equations of motion describing non-standard orbits; Section III deals with the motion near the bounce points, where the interaction with the ripple takes place; the onset of stochasticity is discussed in Section IV; numerical results are presented in Section V; finally, our conclusions are given in Section VI.

II. Unperturbed motion

Magnetic field ripple primarily affects particle motion near turning points, i.e. where the parallel velocity $v_{||}$ vanishes. Between turning points, particle orbits are virtually unperturbed. For this reason, the ripple does not interact with passing particles, and needs only to be taken into account near turning points when analysing trapped particle motion. In this Section, we determine the motion of trapped particles unperturbed by ripple, i.e. between turning points. The analysis is similar to that given in Ref.[11], but different variables are employed, and it allows for an orbitary magnitude of the magnetic shear. All finite orbit-width effects are retained.

The magnetic field in a tokamak can be written [12]

$$\mathbf{B} = \frac{1}{2\pi} \nabla \times (\psi_T \nabla\theta - \psi_P \nabla\varphi) \tag{1}$$

where θ and φ are poloidal and toroidal angles, and ψ_T and ψ_P are the corresponding flux functions. **B** is dominated by the first term representing the toroidal field, which is inversely proportional to the major radius R. The flux surfaces are assumed to be elliptical, and are labelled by the minor radius coordinate

$$r = \sqrt{x^2 + z^2/k^2} \tag{2}$$

Here k is the ellipticity, z denotes the vertical coordinate, and $x=R-R_c$ is the horizontal distance from the magnetic axis, situated at $R=R_c$. The inverse aspect ratio $\varepsilon=r/R$ is, as usual, taken to be small, and the safety factor $q=d\psi_T/d\psi_P$ is approximately equal to

$$q = \frac{2\pi k B r}{d\psi_P/dr} \tag{3}$$

since the toroidal flux through a flux surface is $\psi_T \approx k\pi r^2 B$.

For describing particle orbits in the magnetic field thus defined, we need the following three constants of motion

$$v = \sqrt{2E/m} \tag{4}$$

$$\lambda = \mu B(R_c)/E - 1 = (1-\chi^2)\, x/R_c - \chi^2 \tag{5}$$

$$J = -p_\varphi/mvR_c \approx \psi - \chi R/R_c \tag{6}$$

derived from the kinetic energy E, the magnetic moment μ, and the toroidal momentum p_φ. Here, v is the velocity, $\chi = v_\parallel/v$, ψ is the normalized poloidal flux

$$\psi = \omega_c \psi_P / 2\pi v R_c, \tag{7}$$

and ω_c is the cyclotron frequency. The variable ψ, which will be used for describing the radial position of the particle along the orbit, is related to the minor radius r by

$$r^2(\psi) = \frac{2vR_c}{k\omega_c} \int_0^\psi q(\psi')\, d\psi' \tag{8}$$

as follows from Eq.(3). For convenience, we shall in the following assume that q is a linear function of ψ

$$q(\psi) = q_0 + q_1 \psi \tag{9}$$

so that

$$r^2(\psi) = \frac{vR_c}{k\omega_c}(2q_0\psi + q_1\psi^2). \tag{10}$$

The three constants of motion (4)-(6), together with (10) completely determine the shape of the orbit. In fact, λ and J define the horizontal and radial position of the bounce point (χ=0) of trapped particles, and relate x to ψ along the orbit; from Eqs (5) and (6) we have (to the lowest order in ε)

$$x = \frac{R_c}{1-\lambda}[\lambda + (\psi - J)^2] \tag{11}$$

Combined with Eq.(2), this yields

$$\frac{z^2(\psi)}{k^2} = r^2(\psi) - \left(\frac{R_c}{1-\lambda}\right)^2[\lambda + (\psi-J)^2]^2 = \left(\frac{R_c}{1-\lambda}\right)^2(\psi_1-\psi)(\psi-\psi_2)(\psi-\psi_3)(\psi-\psi_4) \tag{12}$$

where ψ_i are the roots of the quartic polynomial $z^2(\psi)$, indicating where the trajectory crosses the equatorial plane z=0. They are most easily pictured in the (x,ψ)-plane, where they are determined by the points of intersection between the curves (10) and (11) (with R=x in the former equation), cf Refs [11,13,14]. For trapped particles, there are two real roots ψ_1 and ψ_2 such that $\psi_2 < J < \psi_1$, which by virtue of (6) implies that $v_{\|}(\psi_2) < 0 < v_{\|}(\psi_1)$.

The drift velocity

$$v_d = -\frac{v^2(1+\chi^2)}{2\omega_c R}\nabla z \approx -\frac{(1-\lambda)\,v^2}{2\omega_c R_c}\nabla z \tag{13}$$

makes the trajectory deviate from the magnetic field lines, and causes ψ to vary in time according to

$$\dot{\psi} = \mathbf{v}_d \cdot \nabla\psi = -\frac{(1-\lambda)}{2qR_c^2}\frac{z}{k} = \pm\frac{v}{2q(\psi)R_c}\sqrt{(\psi_1-\psi)(\psi-\psi_2)(\psi-\psi_3)(\psi-\psi_4)} \quad (14)$$

where we have used Eqs (2), (8) and (12). This equation of motion (14), together with the relations (9)-(11) which define the shape of the orbit, completely determine the motion of a particle. In order to obtain the position of the particle as a function of time, one must factorize the quartic polynomial $z^2(\psi)$, Eq. (11), and solve the differential equation (14). This is most easily accomplished in the limits of low and high energies. At low energies, the orbit topology is well known: the banana width is small in comparison with r, and all ψ_i are close to J. The high-energy limit has previously been discussed by Stringer [15], Goloborod'ko *et al.* [16], and Porcelli *et al.* [17]. Because of the large drift velocity (13), the banana width becomes very large $\psi_1 >> \psi_2$, so that in the equation for ψ_1 we can consider the orbit as passing through the magnetic axis. This means that the constant term in the polynomial (12) almost vanishes, $\lambda + J^2 \approx 0$, and the equation for ψ_1 becomes

$$\psi^3 - 4J\psi^2 + 4J^2\psi - \frac{v}{k\omega_c R_c}(q_1\psi + 2q_0) = 0 \quad (15)$$

At sufficiently high energies, this equation is further simplified since $\psi_1 >> J$, and the two middle terms in (15) drop out. If, in addition, the magnetic shear is small ($q_1\psi << 2q_0$), the equation becomes trivial

$$\psi^3 = \frac{2q_0 v}{k\omega_c R_c} \quad (16)$$

The bounce time is easily evaluated in this limit. As seen from Eqs (14) and (16), it becomes

$$\tau_b = 2\int_{\psi_2}^{\psi_1} \frac{d\psi}{\dot{\psi}} = \frac{4q_0R_c}{v}\int_0^{\psi_1} \frac{d\psi}{\sqrt{\psi(\psi_1^3-\psi^3)}} = \frac{\pi^{1/3}\,\Gamma(7/6)}{\Gamma(2/3)}\left(\frac{4k\omega_cR_c}{q_0v}\right)^{4/3}\frac{q_0^2}{k\omega_c} \qquad (17)$$

quite independently of λ and J.

In the following, we shall also need the angle $\Delta\varphi$ between two successive bounce points. It is most easily obtained by integrating

$$\dot{\varphi} \approx \chi v/R_c \approx (\psi - J)\, v/R_c \qquad (18)$$

with respect to time using Eq.(14):

$$\Delta\varphi = 4\int_J^{\psi_i} \frac{q(\psi)\,|\psi - J|\,d\psi}{\sqrt{(\psi_1-\psi)(\psi-\psi_2)(\psi-\psi_3)(\psi-\psi_4)}} \qquad (19)$$

where i=1 for the outer branch of the orbit, and i=2 for the inner branch.

III. Motion near the bounce points

Having established the relevant features of unperturbed particle motion, we now turn our attention to the interaction with the magnetic field ripple, taking place in the vicinity of the bounce points. As is well known, the ripple causes a particle to take a vertical step at the turning point, conserving v and λ, but not J. In this Section, we shall calculate the step size ΔJ paying particular attention to the effects of finite Larmor radius and possible non-localization of the resonance. The ripple field is taken to be of the form [6]

$$\tilde{\mathbf{B}} = B_0\,[\delta_x(x,z)\sin N\varphi\,\nabla x + \delta_z(x,z)\sin N\varphi\,\nabla z + \delta(x,z)\cos N\varphi\, R\nabla\varphi] \qquad (20)$$

where B_0 is the background magnetic field strength, and N>>1 is the number of toroidal field coils. The corresponding vector potential can be written

$$\tilde{\mathbf{A}} = A_x \nabla x + A_z \nabla z \tag{21}$$

since a suitable gauge transformation can be applied to eliminate any toroidal component of $\tilde{\mathbf{A}}$. From $\nabla \times \tilde{\mathbf{A}} = \tilde{\mathbf{B}}$ it then follows

$$\frac{\partial A_x}{\partial \varphi} = \delta_z R B_0 \sin N\varphi \ , \quad \frac{\partial A_z}{\partial \varphi} = -\delta_x R B_0 \sin N\varphi \tag{22}$$

In the guiding-centre approximation, the particle motion is described by the Lagrangian [18]

$$L = \frac{1}{2} m v_{\|}^2 + \frac{e}{c} \mathbf{v} \cdot \mathbf{A} - \mu B \tag{23}$$

Because of the presence of magnetic field ripple breaking toroidal symmetry, the toroidal momentum $p_\varphi = \partial L / \partial \dot{\varphi}$ is not conserved, and varies in time according to

$$\dot{p}_\varphi = \partial L / \partial \varphi = m v_{\|} \, \mathbf{v} \cdot \frac{\partial (\mathbf{B}/B)}{\partial \varphi} + \frac{e}{c} \, \mathbf{v} \cdot \frac{\partial \mathbf{A}}{\partial \varphi} - \mu \frac{\partial B}{\partial \varphi} \tag{24}$$

Integrated over time in the vicinity of a bounce point, this gives the radial step taken by a particle due to the influence of the ripple. The dominant contribution comes from the last term, giving

$$\Delta p_\varphi = \mu N B_0 \int \delta(x,z) \sin N\varphi \, dt \tag{25}$$

If N is large, and $\delta(x,z)$ is approximately constant over the extent of the bounce point (to be defined below), this integral can be evaluated by means of the stationary-phase method. We then find

$$\Delta p_\varphi = \mu\delta B_0\sqrt{2\pi N/|\ddot{\varphi}_b|}\,\sin(N\varphi_b+\sigma\pi/4)\ ,\quad \sigma=\ddot{\varphi}_b/|\ddot{\varphi}_b| \tag{26}$$

where $\varphi=\varphi_b$ is the location of the bounce point, and $\ddot{\varphi}_b$ is the toroidal acceleration there. The latter is obtained by differentiating Eq.(18) with respect to time and using (14)

$$\ddot{\varphi}_b = -\frac{v^2}{2qR_c^3}\frac{z}{k} \tag{27}$$

Combining the last two expressions and dividing by $-mvR_c$, we then get the jump in J taken by the particle at the bounce point

$$\Delta J = \delta\left(\frac{N\pi qkR_c}{z}\right)^{1/2}\sin(N\varphi_b+\sigma\pi/4) \tag{28}$$

This result can be found in most earlier studies of ripple diffusion, e.g. Refs [1,4,6]. In deriving it, a number of approximations have been made: The ripple amplitude δ has been assumed to be sufficiently small so that the unperturbed value of $\ddot{\varphi}_b$ (27) can be used; corrections for finite δ can be found in Refs [4,6] (These are mainly important for bounce points near the horizontal plane z=0.). Furthermore, the first two terms in (24) have been disregarded, and, most importantly, the variation in $\delta(x,z)$ near the bounce point has been neglected. Let us investigate these approximations more closely. We start by justifying the neglect of the two first terms in Eq.(24). The first one is readily seen to be small since

$$\frac{\mathbf{B}}{B}=\frac{\mathbf{B}_0+\tilde{\mathbf{B}}}{|\mathbf{B}_0+\tilde{\mathbf{B}}|}=\frac{\mathbf{B}_0}{B_0}+\frac{\tilde{\mathbf{B}}_p}{B_0}+O(\delta^2) \tag{29}$$

where $\tilde{\mathbf{B}}_p$ is the poloidal component of $\tilde{\mathbf{B}}$, and hence

$$mv_{\|}\mathbf{v}\cdot\partial(\mathbf{B}/B)/\partial\varphi \sim mv_{\|}\mathbf{v}\cdot\mathbf{B}_p N\delta/B << \mu\,\partial B/\partial\varphi \tag{30}$$

The second term in (24) can, by using (22), be written

$$\frac{e}{c}\mathbf{v}\cdot\frac{\partial\mathbf{A}}{\partial\varphi}=\frac{eRB_0}{c}\,(\dot{x}\delta_z-\dot{z}\delta_x)\sin N\varphi \tag{31}$$

Here, the horizontal and vertical velocities $\dot{x}$ and $\dot{z}$ can be expressed in terms of $\dot{\varphi}$

$$\begin{aligned}\dot{x}&=\mathbf{v}_{\|}\cdot\nabla x=\frac{v_{\|}}{2\pi B}\,(\nabla\varphi\times\nabla\psi_P)\cdot\nabla x=\dot{\varphi}z/qk\\ \dot{z}&=\mathbf{v}_{\|}\cdot\nabla z-v_d=\dot{\varphi}kx/q-v_d\end{aligned} \tag{32}$$

where we have used the unperturbed orbit equations (1), (2), (3), and (6). Combining (31) and (32), we then have

$$\frac{e}{c}\mathbf{v}\cdot\frac{\partial\mathbf{A}}{\partial\varphi}=m\omega_c\left[v_dR_c\delta_x-\frac{\dot{\varphi}R_c}{q}\left(kx\delta_x+\frac{z\delta_z}{k}\right)\right]\sin N\varphi \tag{33}$$

In this expression, the first term can immediately be compared with $-\mu\partial B/\partial\varphi$ in (24), and is found to be small. The second term makes no contribution to Δp_φ since it is a total derivative with respect to time, provided the factor $(kx\delta_x+z\delta_z/k)$ is constant in the region of interaction near the bounce point. Thus, Eq.(33) representing the second term in (24) is negligible, at least as long as the interaction is well localized, an assumption we already have made use of in (26). Let us therefore estimate the extent of the interaction region. From (26), we see that the time during which the interaction takes place is roughly

$\Delta t = \sqrt{2\pi/N|\ddot{\varphi}_b|}$. Substituting here the value of $\ddot{\varphi}_b$ from (27), and using (32) gives an estimate of the distance travelled by the particle whilst interacting with the ripple

$$\Delta x = \pi z/qkN$$

$$\Delta z = \pi kx/qN - \rho\sqrt{\pi qkR/Nz} \qquad (34)$$

where $\rho=v/\omega_c$ is the Larmor radius. Eq.(34) defines the extent of the bounce point with respect to ripple interaction. Clearly $\Delta x \ll r$, and for relevant JET parameters we also have $\Delta z \ll r$ over most of the plasma cross-section. However, in order for the interaction to be well localized, the ripple amplitude δ must also be approximately constant over the interaction region. This condition is only marginally satisfied in JET when 16 toroidal-field coils are used. When the interaction is not localized, the picture becomes more complicated. Then, the integral (25) defining the modification of the orbit due to the presence of ripple must be evaluated along the entire trajectory, taking into account the detailed variation of $\delta(x,z)$ along it. This is, however, beyond the scope of the present analysis.

Above, we have used the guiding-centre approximation, neglecting any finite-Larmor-radius variation of magnetic field quantities. However, because of the low magnetic field strength (B=1.4 T) at JET when only 16 toroidal-field coils are in use, a typical Larmor radius is quite large, ρ=10 cm for a 1 MeV proton. In fact, over the diameter 2ρ, the ripple amplitude δ varies by a factor of about 3, cf Fig.2. This calls for a more exact analysis of the ripple-induced perturbation of particle orbits. For this purpose, let us consider the exact Lagrange function, governing charged particle motion

$$L = \frac{1}{2}mv^2 + \frac{e}{c}\mathbf{v}\cdot\mathbf{A} \qquad (35)$$

where $\mathbf{v}$ now denotes the full velocity of the particle, not that of the guiding centre. The toroidal momentum p_φ corresponding to this Lagrangian coincides to all orders in ρ/R with that of the guiding centre used above [18], and varies, of course, in time as

$$\dot{p}_\varphi = \partial L/\partial\varphi = \frac{e}{c}\,(\mathbf{v}_\parallel + \mathbf{v}_d + \mathbf{v}_L)\cdot\frac{\partial \mathbf{A}}{\partial\varphi} \tag{36}$$

where $\mathbf{v}_L$ refers to the Larmor rotation. Averaging its contribution to $\dot{p}_\varphi$ over a cyclotron period, and using Stoke's theorem, we find

$$<\frac{e}{c}\,\mathbf{v}_L\cdot\frac{\partial \mathbf{A}}{\partial\varphi}> = \frac{\omega_c e}{2\pi c}\,\frac{\partial}{\partial\varphi}\int \mathbf{A}\cdot d\mathbf{l} = -\mu\,\frac{\partial \bar{B}}{\partial\varphi} \tag{37}$$

where $\bar{B}$ denotes the average value of B inside the Larmor circle. Thus, if the Larmor-circle average ripple $\bar{\delta}$ is used instead of that at the guiding centre, all expressions derived above are still valid.

IV. Onset of stochasticity

Eq.(19) in Section II above describes the motion (in the toroidal direction) of particles between bounce points, and Eq.(28) the orbit modification at the turning points. The combination of these results results in a well-known set of finite difference equations [1,4,6] describing the evolution of particle trajectories on long time-scales. If the ripple amplitude is large enough, the vertical steps taken at successive bounce points become decorrelated, randomizing the motion and leading to diffusive loss of the particles. The onset of stochastic motion cannot be accurately predicted by present-day theory, but is known to occur approximately when the following inequality is satisfied

$$\gamma = N\,\Delta J\,\partial(\Delta\varphi)/\partial J > 1 \tag{38}$$

for any single step of the mapping [1,4,6,19]. Since ΔJ is proportional to the ripple amplitude, this yields a critical ripple amplitude at the bounce point, δ_{crit}, above which stochastic ripple diffusion sets in.

In the small banana-width limit (i.e. at low energies), $\Delta\varphi$ can be calculated analytically. It is equal to [6]

$$\Delta\varphi = \pm 2q\theta_b + \frac{2^{5/2}q^2 v_d}{k\varepsilon^{3/2}v}\left\{E(\kappa) - \frac{K(\kappa)}{2} + \frac{2r}{q}\frac{dq}{dr}\left[E(\kappa) - K(\kappa)\cos^2\frac{\theta_b}{2}\right]\right\} \qquad (39)$$

where the first (usually dominant) term comes from bounce motion following the magnetic field line, and the other arises because of toroidal precession. θ_b is the poloidal angle of the bounce point, $\kappa=\sin\theta/2$, and E and K are complete elliptic integrals. The second term in (39) vanishes in the zero orbit-width limit; in this case the combination of Eqs (38) and (39) results in the following critical ripple amplitude

$$\delta_{crit} = \left(\frac{\varepsilon}{\pi N q}\right)^{3/2}\frac{k}{\rho\, dq/dr} \qquad (40)$$

first derived by Goldston, White and Boozer in Ref.[1]. The factor k accounting for the ellipticity was introduced by Kolesnichenko and Yakovenko [4].

V. Numerical results

When the orbit width is large, no simple analytic expression exists for $\Delta\varphi$, and the full orbit expression (FOE) (19) must be integrated numerically. In this Section, we illustrate the resulting stochastization threshold, and make a comparison with the corresponding small banana width expression (SBWE) which follows from Eq.(39). As mentioned in

the introduction, we use parameters relevant to the recent ripple experiments on JET, summarized in Table 1.

In Fig. 1a, the critical ripple amplitudes δ_{crit} required for stochastization of a 1 MeV hydrogen ion obtained from the FOE and the SBWE are shown. The (negative logarithm of the) critical ripple is plotted as a function of the vertical position of the trapped ion turning point z_{tp} (where $v_{||}=0$), while the horizontal turning point position is kept constant, x_{tp} = -0.4 m. Fig.1b shows where the inner and outer branches of the orbit intersect the horizontal midplane z=0. As expected, the results from the FOE and the SBWE agree at large turning point radii, where the orbit width is smaller than the distance from the magnetic axis and the small banana-width approximation holds. However, near the midplane the deviation between the results becomes significant. The reason for this is that the SBWE for $\partial(\Delta\varphi)\partial J$ as obtained by differentiating Eq.(39) with respect to J diverges as $z_{tp}\rightarrow 0$. This leads to an underestimate of the stochastization threshold in the small banana-width approximation. The difference between δ_{crit} as obtained by the FOE and the SBWE exceeds an order of magnitude for $z_{tp}<0.13$ m Another significant difference occurs around $z_{tp}=0.3$ m Here, the orbits, which are non-standard, are close to the pinch orbit [7] where a sudden transition in orbit topology takes place. As illustrated in Fig.1b, the point where the inner branch of the orbit intersects the midplane moves abruptly from the high-field side of the torus to the low-field side. Figs 2a and 2b illustrate this phenomenon by depicting one orbit just before the transition and one immediately after, i.e.at a slightly larger value of z_{tp}. The "potato" orbit [17] of Fig.2a transforms into the "fat banana" of Fig.2b. Note that both these orbits are trapped in the toroidal direction; $v_{||}$ changes sign not at the tip of the banana, but at the point furthest to the left along the orbit. Stochastization is, naturally, easily achieved in the neighbourhood of the transition region; in fact $\delta_{crit}\rightarrow 0$ at the pinch orbit. It is interesting to note that δ_{crit} is significantly affected in fairly large region; for 0.25 m < z_{tp} < 0.4 m the difference between the FOE and the SBWE is at least a factor of two. It should be pointed out that it

is the behaviour of the inner branch of the orbit that determines the stochastization threshold in this region.

Fig. 3 shows the same as Fig. 1, but with x_{tp}=-0.2 m. The main difference as compared to the case when x_{tp}=-0.4 m is that no pinch orbit exists when x_{tp}=-0.2 m. Instead, the transition from potato shaped orbits to banana orbits is relatively smooth, see Fig.3b. Nevertheless, stochastization is still fairly easily achieved in the transition region, where δ_{crit} is decreased by about an order of magnitude. Fig.4 is again the same plot as Fig.1 but with turning points on the low-field side, x_{tp}=0.1 m. Here, the potato-banana transition is undramatic, and the difference in δ_{crit} obtained from the FOE and the SBWE is only significant near the midplane (for reasons stated above).

A scan in energy for x_{tp}=-0.4 m and z_{tp}=0.2 m is given in Fig.5. Fig.5a shows δ_{crit}, and Fig.5b indicates where the trajectories intersect the midplane. As can be seen, the deviation between the full-orbit and the small banana-width results is quite significant even for relatively modest energies, i.e. for 100-200 keV. Again, a large difference is seen around the transition region between potato-shaped and banana-shaped orbits, and $\delta_{crit}\rightarrow 0$ at the pinch orbit. For higher energies, the curves from the FOE and the SBWE diverge. The reason for this is mainly that the toroidal precession scales differently for non-standard and banana orbits.

The level surfaces of the ripple amplitude in JET when 16 toroidal field coils are in use are shown in Fig.6, and in Fig.7 the corresponding level surfaces of the stochastization parameter γ, Eq.(38), for a 1 MeV hydrogen ion are indicated. Particles having their turning points outside the curve γ=1 suffer stochastic ripple diffusion. In spite of the large differences in δ_{crit} reported above, the level curves from the FOE do not differ much from those of the SBWE. There is a difference near the midplane, where the FOE shows a narrow non-stochastic region for x_{tp}<-0.2 m. Furthermore, the FOE predicts a somewhat smaller non-stochastic region than the SBWE does close the the prompt-loss

boundary around x_{tp}=-0.4 m, z_{tp} = 0.4 m. The reason for the small differences is that the ripple amplitude is large in in the regions where the significant discrepancies in δ_{crit} described above appear. In other words, most of the regions of interest are stochastic anyway. In addition, the ripple gradients are large, so that large differences in δ_{crit} only lead to moderate differences in the number of stochastically moving particles.

VI. Conclusions

In summary, we have found that the non-standard orbit topology of high-energy ions leads to significant (order-of-magnitude) modifications of the Goldston-White-Boozer stochastization threshold [1,4,5,6] for JET-relevant parameters. Particles following orbits with turning points on the high-field side of the torus are most severly affected. In particular, trajectories close to the pinch orbit are very sensitive to the presence of magnitic field ripple. Because of the steepness of the ripple gradient and the largeness of the ripple amplitude, the number of particles suffering stochastic ripple diffusion is only moderately affected by large orbit-width effects.

Some other finite orbit-width effects may also be of importance. The diffusion coefficient for ripple-diffusing particles is inversely proportional to the bounce time, whose value is determined by Eq.(17) rather than by the standard expression. If the ripple-particle resonance is not well localized as discussed in Section III, the step size taken by the particles at the turning points will be affected. This will, of course, also affect the diffusion coefficient.

Acknowledgements

We would like to thank Dr S. Putvinskii for a very useful discussion, and Dr B. Tubbing for providing the JET ripple profile. One of the authors (P.H.) would like to acknowledge the hospitality of the JET Theory Division.

References

[1] GOLDSTON, R.J., WHITE R.B., BOOZER, A.H., Phys. Rev. Lett. **47** (1981) 647.

[2] SADLER, G., et al., in 1992 International Conference on Plasma Physics (Proc. 19th EPS Conference on Controlled Fusion and Plasma Physics, Innsbruck, 1992), Vol. 16C, Part I, European Physical Society (1992) 167.

[3] ZWEBEN, S.J., HAMMETT, G.W., BOIVIN, R.L., PHILIPS, C.K., WILSON, R.J., Nucl. Fusion **32** (1992) 1823; BOIVIN, R., Measurements of Charged Fusion Product Diffusion in TFTR, PhD Thesis, Rep. PPPL-2797, Princeton Plasma Physics Laboratory, Princeton, NJ, USA (1991).

[4] KOLESNICHENKO YA.I., YAVORSKIJ, V.A., Nucl. Fusion **29** (1989) 1319.

[5] GRUA, P., ROUBIN J.-P., Nucl. Fusion **30** (1990) 1499.

[6] YUSHMANOV, P.N., in Reviews of Plasma Physics, Vol. 16, Consultants Bureau, New York, 1990.

[7] PENG, Y-K.M., ROME, J.A., Nucl. Fusion **19** (1979) 1193.

[8] TANI, K., TAKIZUKA, T, AZUMI, M., KISHIMOTO, H., Nucl. Fusion **23** (1983) 657.

[9] HIVELY, L.M., Nucl. Fusion **24** (1984) 779.

[10] PUTVINSKII, S., Private communication (1992).

[11] HELANDER, P., LISAK, M., Phys. Fluids B4 (1992) 1927.

[12] HAZELTINE, R.D., MEISS, J.D., Plasma Confinement, Addison-Wesley, Redwood City, USA, 1992.

[13] PUTVINSKII, S.V., Sov. J. Plasma Phys. **14** (1988) 729.

[14] PUTVINSKII, S.V., Sov. J. Plasma Phys. **15** (1989) 73.

[15] STRINGER, T.E., Plasma Physics **16** (1974) 651.

[16] GOLOBOROD'KO, V.YA., KOLESNICHENKO, YA.I., YAVORSKIJ, V.A., Nucl. Fusion **23** (1981) 399.

[17] PORCELLI, F., STANKIEWICZ, R., BERK, H.L., ZHANG, Y.Z., Phys. Fluids B4 (1992) 3017.

[18] LITTLEJOHN, R.G., J. Plasma Phys. **29** (1983) 111.

[19] SAGDEEV, R.Z., USIKOV, D.A., ZASLAVSKY, G.M., Nonlinear Physics - From the Pendulum to Turbulence and Chaos, Academic, New York, 1988.

major radius, R	3.0 [m]
magnetic field at the axis, B_o	1.4 [T]
safety factor at the axis, q_o	0.8
safety factor at the boundary, q_a	3.0
ellipticity, k	1.4

Table 1: Parameters relevant to the JET ripple experiment.

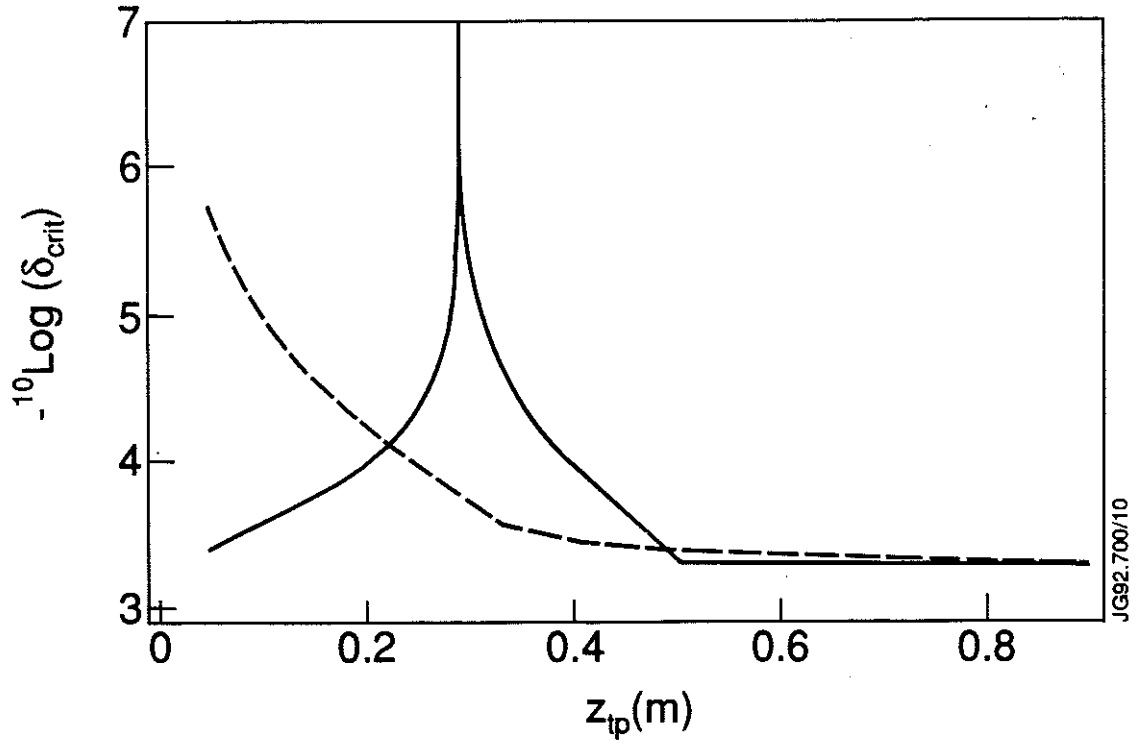

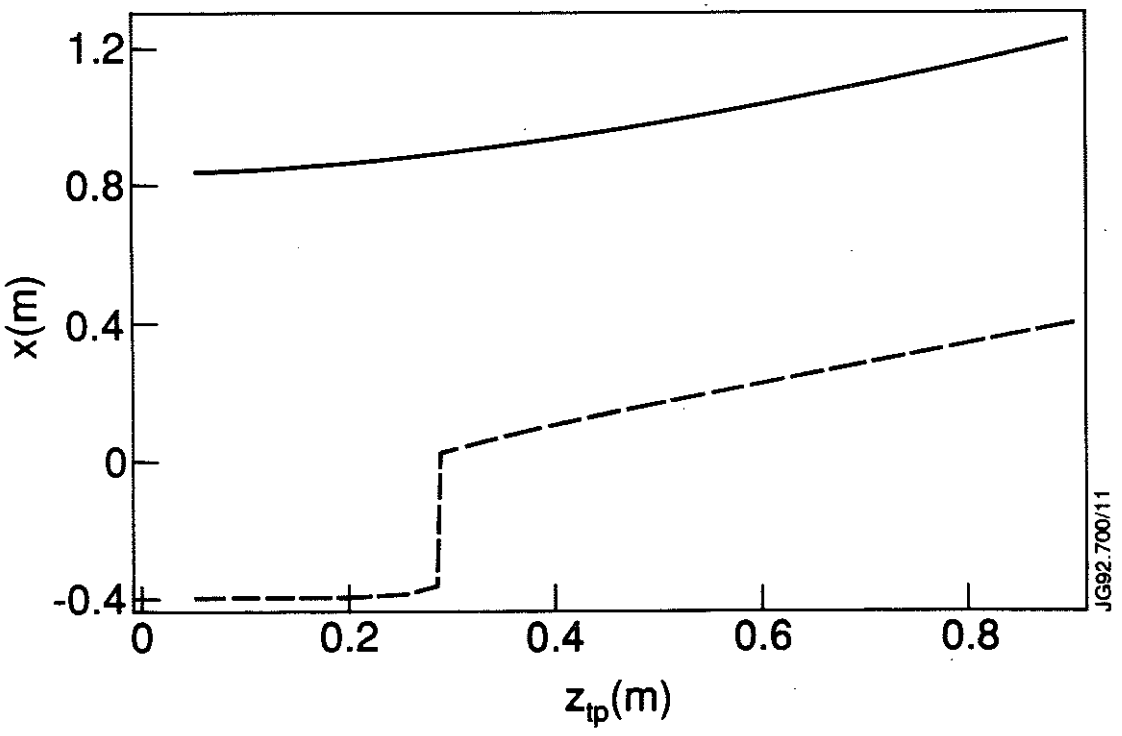

Fig.1. $-^{10}\log \delta_{crit}$, full orbit expression solid line, small banana width expression dashed line, (a); and the points of intersection with the midplane, outer branch solid line, inner branch dashed line, (b) for a 1 MeV proton at x_{tp} = -0.4 m in JET when 16 TF coils are in use

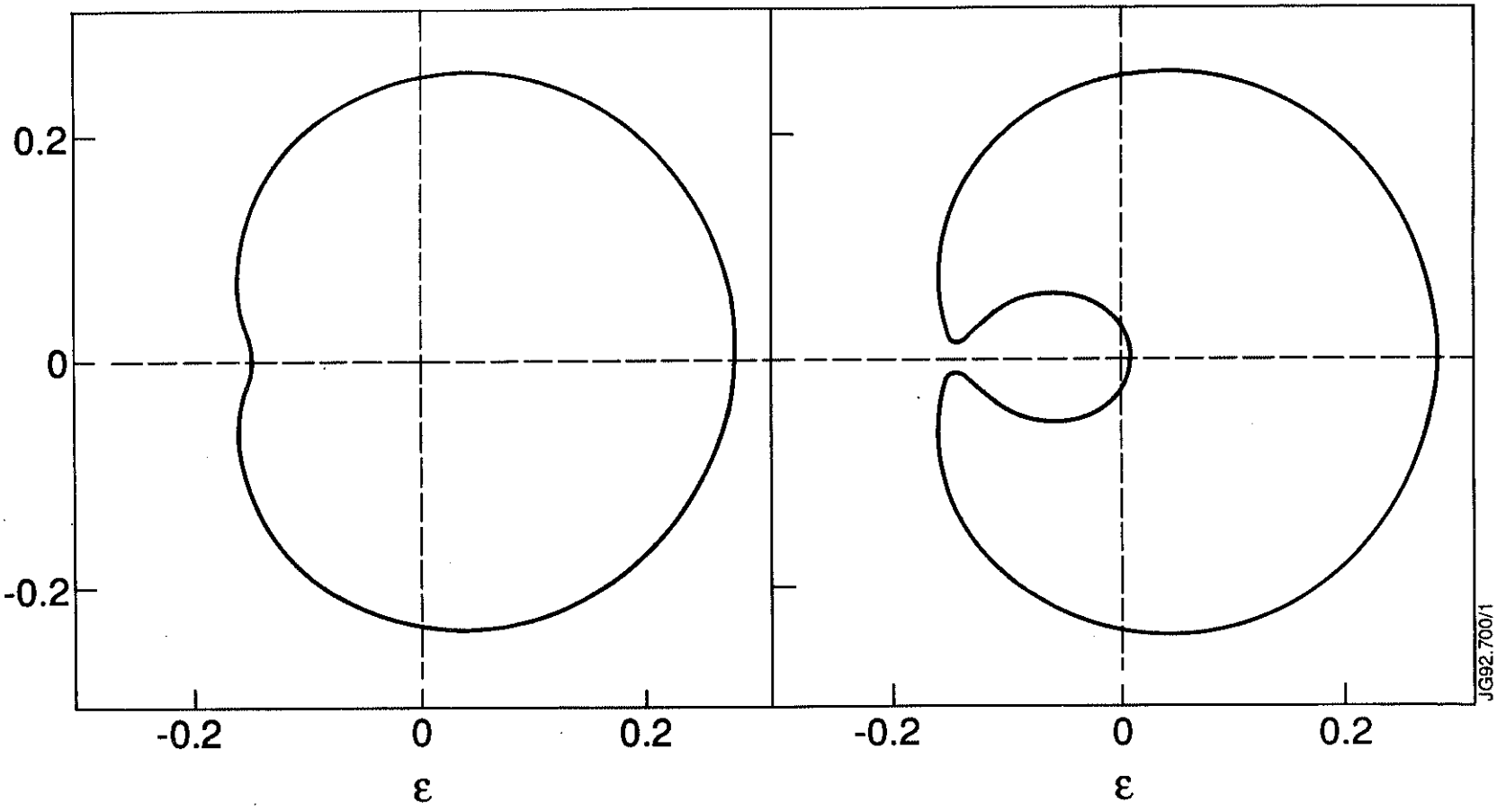

Fig.2. Potato (a) and banana (b) orbits close to the pinch orbit.

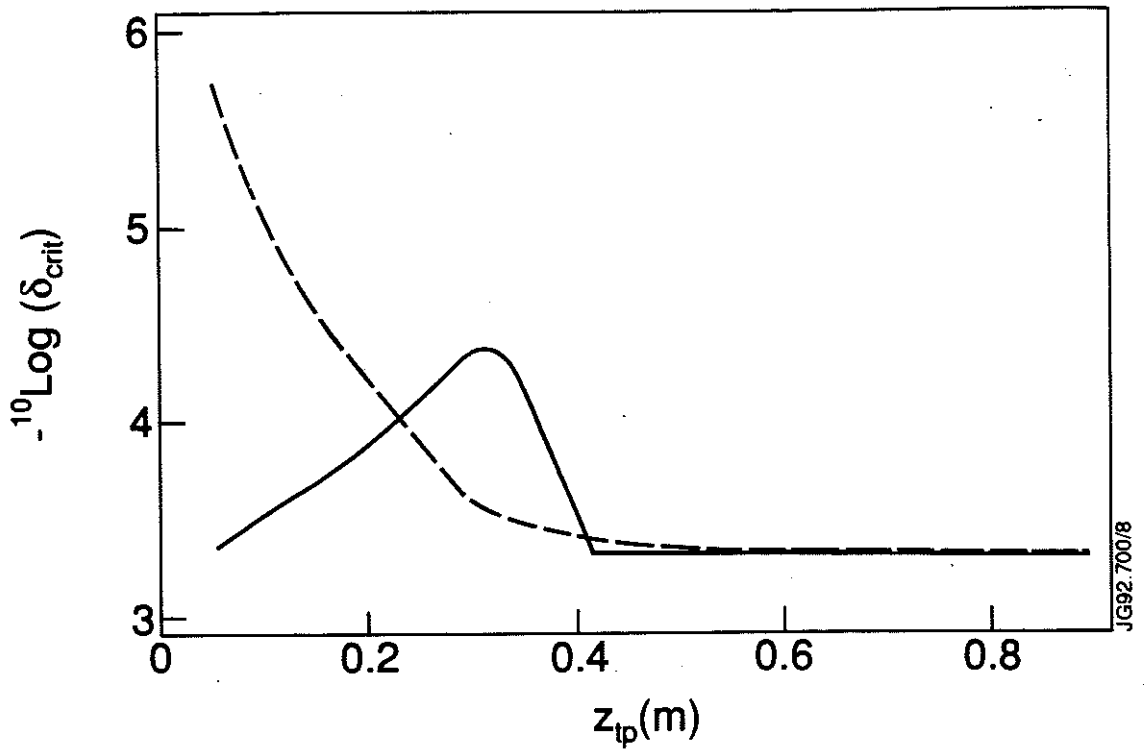

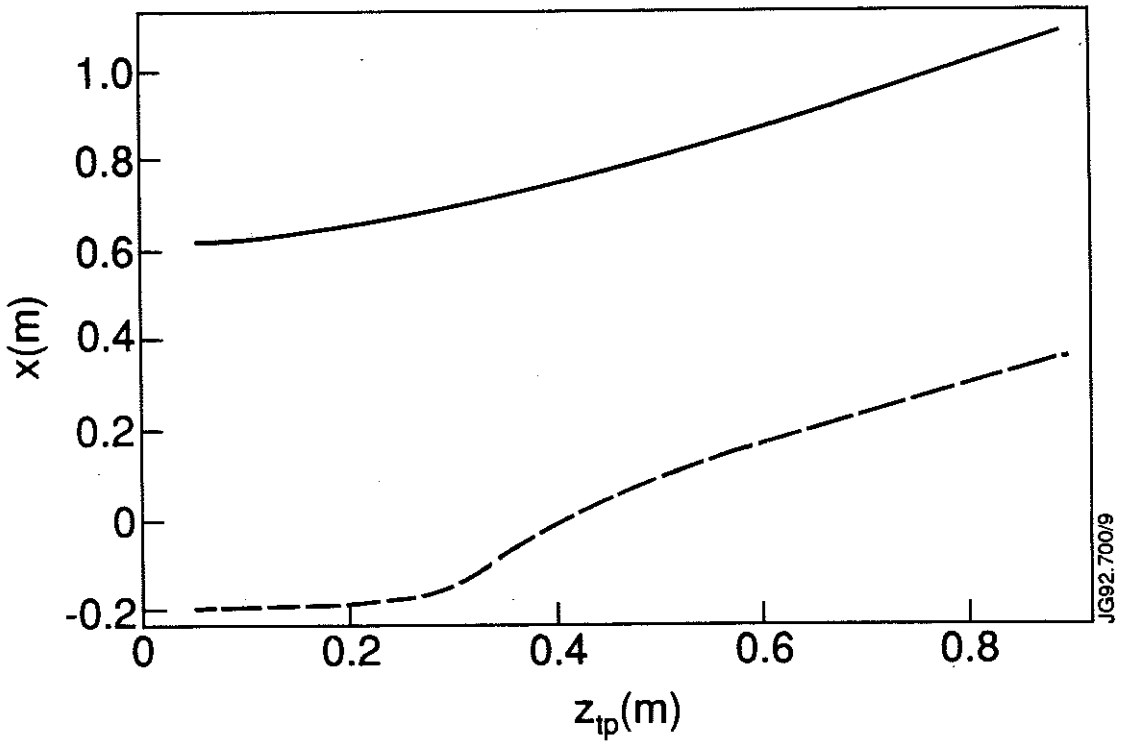

Fig.3. $-^{10}\log \delta_{crit}$, full orbit expression solid line, small banana width expression dashed line, (a); and the points of intersection with the midplane, outer branch solid line, inner branch dashed line, (b) for a 1 MeV proton at $x_{tp} = -0.2$ m in JET .

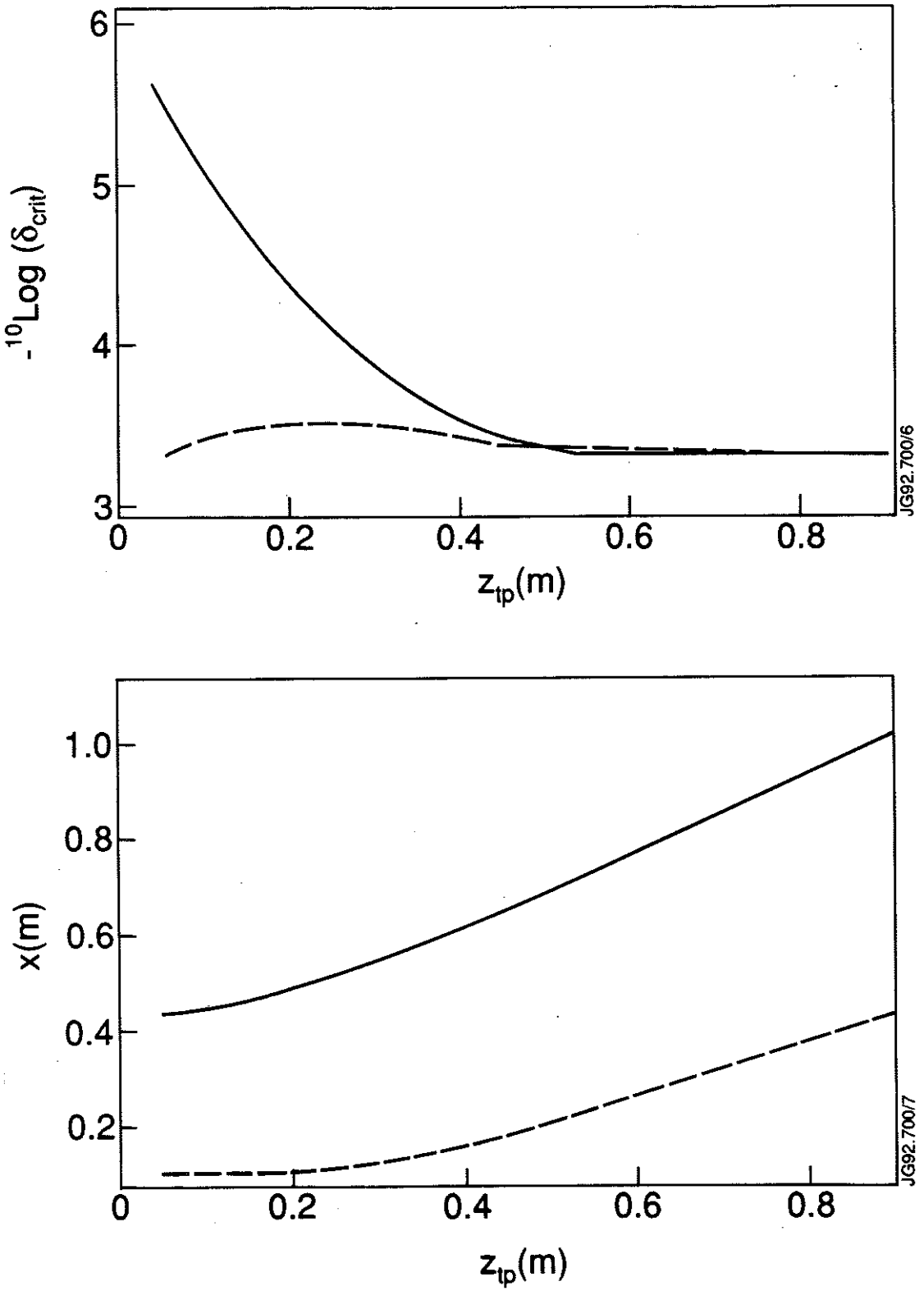

Fig.4. $-^{10}\log \delta_{crit}$, full orbit expression solid line, small banana width expression dashed line, (a); and the points of intersection with the midplane, outer branch solid line, inner branch dashed line, (b) for a 1 MeV proton at $x_{tp} = 0.1$ m in JET .

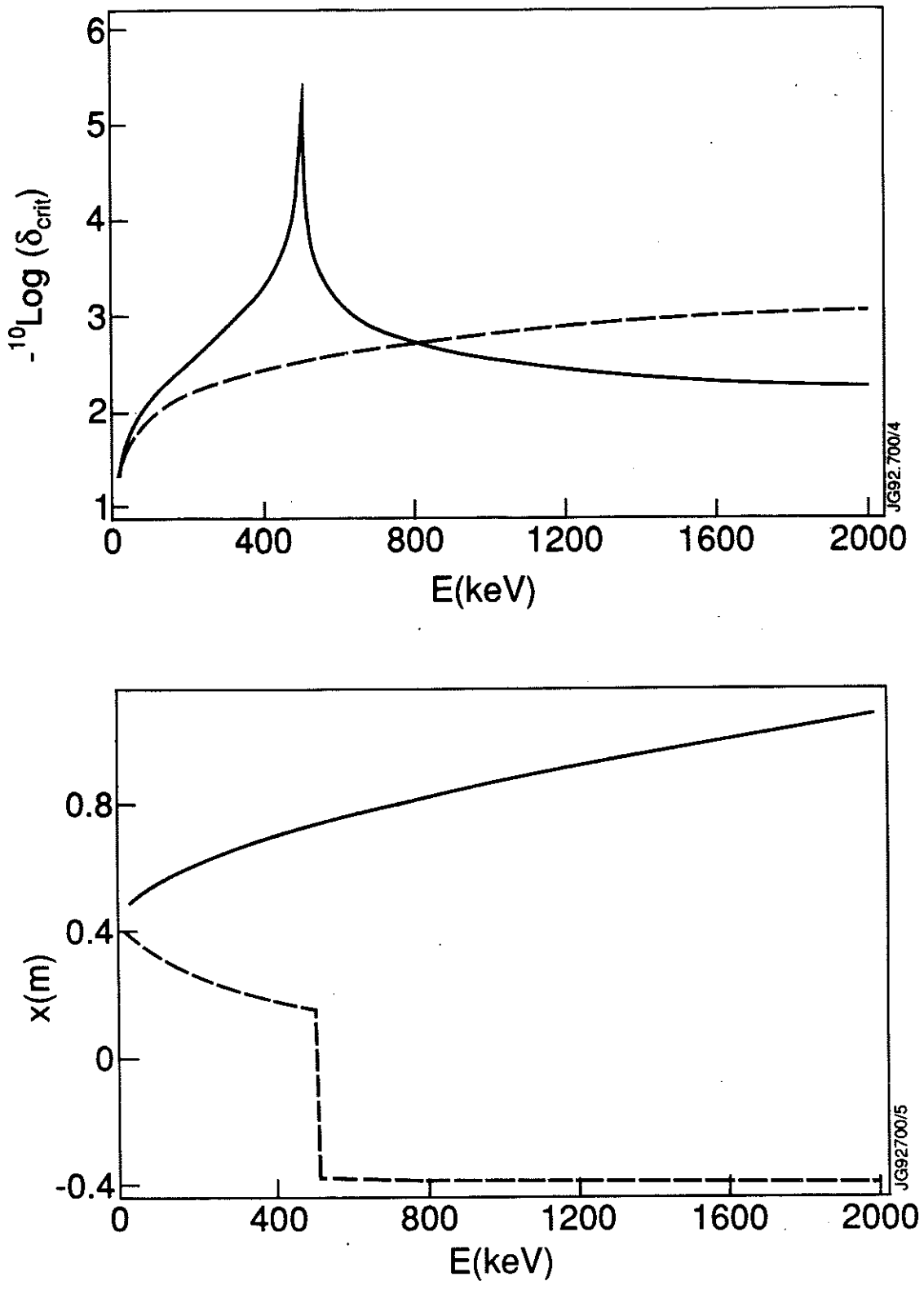

Fig.5. $-^{10}\log \delta_{crit}$, full orbit expression solid line, small banana width expression dashed line, (a); and the points of intersection with the midplane, outer branch solid line, inner branch dashed line, (b) for a proton at x_{tp} = -0.2 m, z_{tp}=0.2 m in JET.

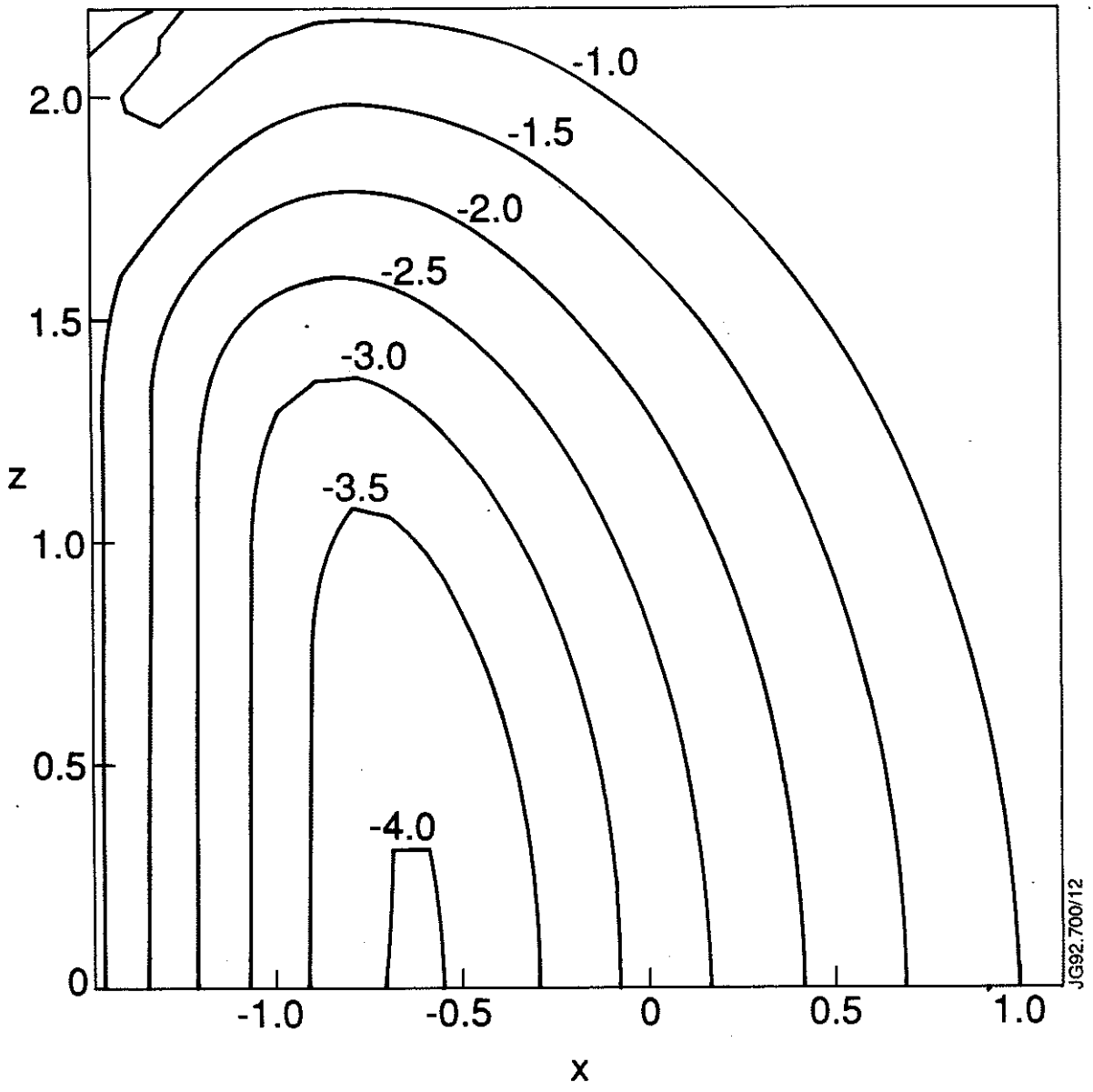

Fig.6. The ripple profile in JET when 16 TF coils are in operation, the numbers labelling the level curves are $^{10}\log \delta$.

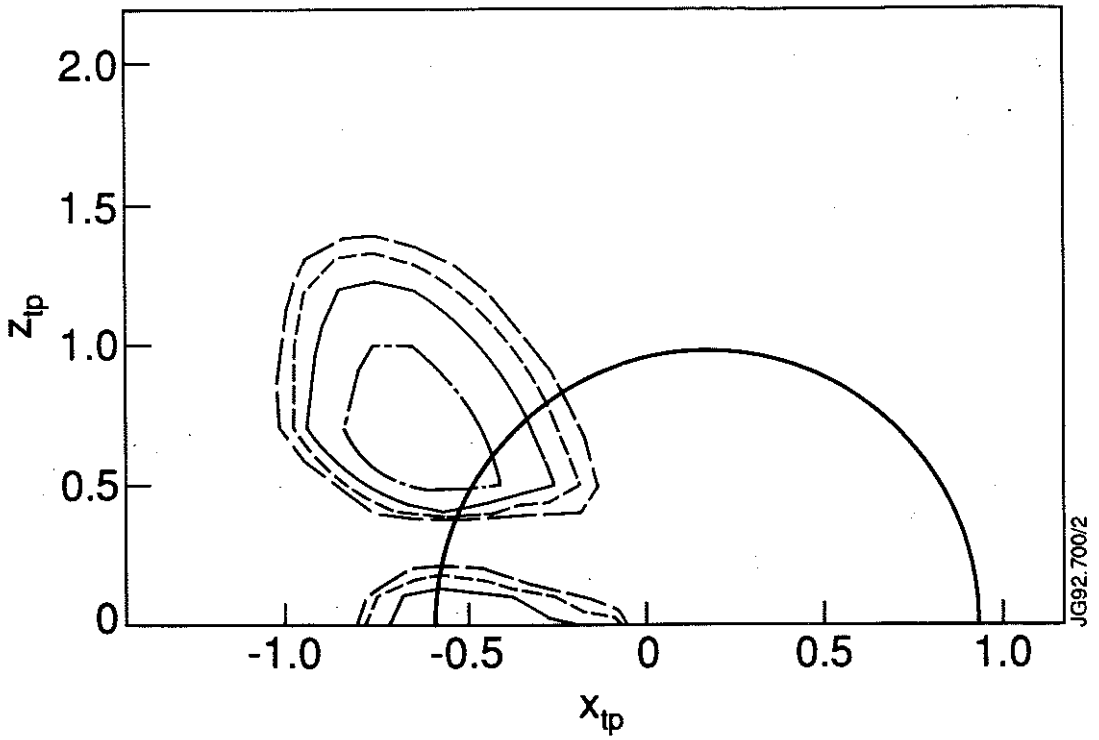

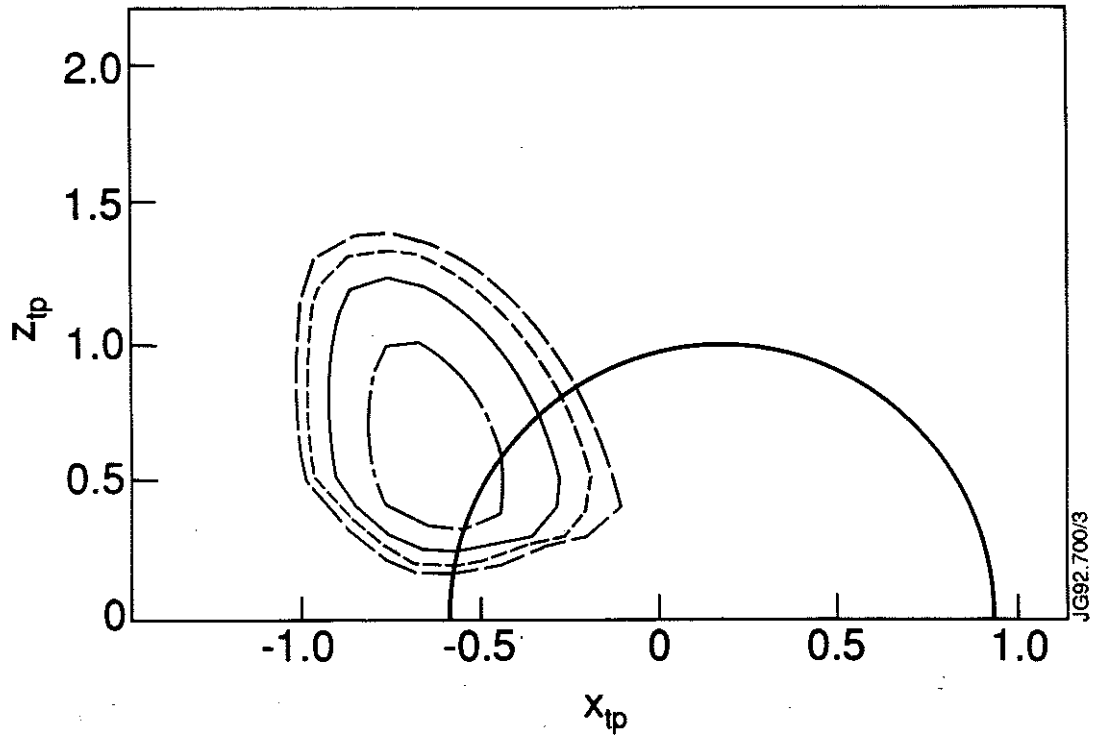

Fig.7. Level curves of the stochastization parameter (38) full orbit expression (a); small banana width expression (b) for a 1 MeV proton in JET. The promt loss boundary is marked with a bold solid line and $\gamma = 0.5$ (–·–·–), $\gamma = 1.0$ (——), $\gamma = 1.5$ (- - - -), $\gamma = 2.0$ (– – – –).

Appendix I

THE JET TEAM

JET Joint Undertaking, Abingdon, Oxon, OX14 3EA, U.K.

J.M. Adams[1], B. Alper, H. Altmann, A. Andersen[14], P. Andrew, S.Ali-Arshad, W. Bailey, B. Balet, P. Barabaschi, Y. Baranov, P. Barker, R. Barnsley[2], M. Baronian, D.V. Bartlett, A.C. Bell, G. Benali, P. Bertoldi, E. Bertolini, V. Bhatnagar, A.J. Bickley, D. Bond, T. Bonicelli, S.J. Booth, G. Bosia, M. Botman, D. Boucher, P. Boucquey, M. Brandon, P. Breger, H. Brelen, W.J. Brewerton, H. Brinkschulte, T. Brown, M. Brusati, T. Budd, M. Bures, P. Burton, T. Businaro, P. Butcher, H. Buttgereit, C. Caldwell-Nichols, D.J. Campbell, D. Campling, P. Card, G. Celentano, C.D. Challis, A.V.Chankin[23], A. Cherubini, D. Chiron, J. Christiansen, P. Chuilon, R. Claesen, S. Clement, E. Clipsham, J.P. Coad, I.H. Coffey[24], A. Colton, M. Comiskey[4], S. Conroy, M. Cooke, S. Cooper, J.G. Cordey, W. Core, G. Corrigan, S. Corti, A.E. Costley, G. Cottrell, M. Cox[7], P. Crawley, O. Da Costa, N. Davies, S.J. Davies[7], H. de Blank, H. de Esch, L. de Kock, E. Deksnis, N. Deliyanakus, G.B. Denne-Hinnov, G. Deschamps, W.J. Dickson[19], K.J. Dietz, A. Dines, S.L. Dmitrenko, M. Dmitrieva[25], J. Dobbing, N. Dolgetta, S.E. Dorling, P.G. Doyle, D.F. Düchs, H. Duquenoy, A. Edwards, J. Ehrenberg, A. Ekedahl, T. Elevant[11], S.K. Erents[7], L.G. Eriksson, H. Fajemirokun[12], H. Falter, J. Freiling[15], C. Froger, P. Froissard, K. Fullard, M. Gadeberg, A. Galetsas, L. Galbiati, D. Gambier, M. Garribba, P. Gaze, R. Giannella, A. Gibson, R.D. Gill, A. Girard, A. Gondhalekar, D. Goodall[7], C. Gormezano, N.A. Gottardi, C. Gowers, B.J. Green, R. Haange, A. Haigh, C.J. Hancock, P.J. Harbour, N.C. Hawkes[7], N.P. Hawkes[1], P. Haynes[7], J.L. Hemmerich, T. Hender[7], J. Hoekzema, L. Horton, J. How, P.J. Howarth[5], M. Huart, T.P. Hughes[4], M. Huguet, F. Hurd, K. Ida[18], B. Ingram, M. Irving, J. Jacquinot, H. Jaeckel, J.F. Jaeger, G. Janeschitz, Z. Jankowicz[22], O.N. Jarvis, F. Jensen, E.M. Jones, L.P.D.F. Jones, T.T.C. Jones, J-F. Junger, F. Junique, A. Kaye, B.E. Keen, M. Keilhacker, W. Kerner, N.J. Kidd, R. Konig, A. Konstantellos, P. Kupschus, R. Lässer, J.R. Last, B. Laundy, L. Lauro-Taroni, K. Lawson[7], M. Lennholm, J.Lingertat[13], R.N. Litunovski, A. Loarte, R. Lobel, P. Lomas, M. Loughlin, C. Lowry, A.C. Maas[15], B. Macklin, C.F. Maggi[16], G. Magyar, V. Marchese, F. Marcus, J. Mart, D. Martin, E. Martin, R. Martin-Solis[8], P. Massmann, G. Matthews, H. McBryan, G. McCracken[7], P. Meriguet, P. Miele, S.F. Mills, P. Millward, E. Minardi[16], R. Mohanti[17], P.L. Mondino, A. Montvai[3], P. Morgan, H. Morsi, G. Murphy, F. Nave[27], S. Neudatchin[23], G. Newbert, M. Newman, P. Nielsen, P. Noll, W. Obert, D. O'Brien, J. O'Rourke, R. Ostrom, M. Ottaviani, S. Papastergiou, D. Pasini, B. Patel, A. Peacock, N. Peacock[7], R.J.M. Pearce, D. Pearson[12], J.F. Peng[26], R. Pepe de Silva, G. Perinic, C. Perry, M.A. Pick, J. Plancoulaine, J-P. Poffé, R. Pohlchen, F. Porcelli, L. Porte[19], R. Prentice, S. Puppin, S. Putvinskii[23], G. Radford[9], T. Raimondi, M.C. Ramos de Andrade, M. Rapisarda[29], P-H. Rebut, R. Reichle, S. Richards, E. Righi, F. Rimini, A. Rolfe, R.T. Ross, L. Rossi, R. Russ, H.C. Sack, G. Sadler, G. Saibene, J.L. Salanave, G. Sanazzaro, A. Santagiustina, R. Sartori, C. Sborchia, P. Schild, M. Schmid, G. Schmidt[6], H. Schroepf, B. Schunke, S.M. Scott, A. Sibley, R. Simonini, A.C.C. Sips, P. Smeulders, R. Smith, M. Stamp, P. Stangeby[20], D.F. Start, C.A. Steed, D. Stork, P.E. Stott, P. Stubberfield, D. Summers, H. Summers[19], L. Svensson, J.A. Tagle[21], A. Tanga, A. Taroni, C. Terella, A. Tesini, P.R. Thomas, E. Thompson, K. Thomsen, P. Trevalion, B. Tubbing, F. Tibone, H. van der Beken, G. Vlases, M. von Hellermann, T. Wade, C. Walker, D. Ward, M.L. Watkins, M.J. Watson, S. Weber[10], J. Wesson, T.J. Wijnands, J. Wilks, D. Wilson, T. Winkel, R. Wolf, D. Wong, C. Woodward, M. Wykes, I.D. Young, L. Zannelli, A. Zolfaghari[28], G. Zullo, W. Zwingmann.

PERMANENT ADDRESSES

1. UKAEA, Harwell, Didcot, Oxon, UK.
2. University of Leicester, Leicester, UK.
3. Central Research Institute for Physics, Budapest, Hungary.
4. University of Essex, Colchester, UK.
5. University of Birmingham, Birmingham, UK.
6. Princeton Plasma Physics Laboratory, New Jersey, USA.
7. UKAEA Culham Laboratory, Abingdon, Oxon, UK.
8. Universidad Complutense de Madrid, Spain.
9. Institute of Mathematics, University of Oxford, UK.
10. Freien Universität, Berlin, F.R.G.
11. Royal Institute of Technology, Stockholm, Sweden.
12. Imperial College, University of London, UK.
13. Max Planck Institut für Plasmaphysik, Garching, FRG.
14. Risø National Laboratory, Denmark.
15. FOM Instituut voor Plasmafysica, Nieuwegein, The Netherlands.
16. Dipartimento di Fisica, University of Milan, Milano, Italy.
17. North Carolina State University, Raleigh, NC, USA
18. National Institute for Fusion Science, Nagoya, Japan.
19. University of Strathclyde, 107 Rottenrow, Glasgow, UK.
20. Institute for Aerospace Studies, University of Toronto, Ontario, Canada.
21. CIEMAT, Madrid, Spain.
22. Institute for Nuclear Studies, Otwock-Swierk, Poland.
23. Kurchatov Institute of Atomic Energy, Moscow, USSR
24. Queens University, Belfast, UK.
25. Keldysh Institute of Applied Mathematics, Moscow, USSR.
26. Institute of Plasma Physics, Academica Sinica, Hefei, P. R. China.
27. LNETI, Savacem, Portugal.
28. Plasma Fusion Center, M.I.T., Boston, USA.
29. ENEA, Frascati, Italy.

At 1st July, 1992